doi: 10.82124/CEAS-GNC-2026-094 CEAS-GNC-2026-094

EuroGNC Navigation Guidance Control CEAS Madrid, Spain May 5th-7th uc3m Universidad Carlos III de Madrid AIAA 2026

Real- vs Complex-valued Data Partitioning for System Identification via Tangential Interpolation

Gabriele Dessena *Juan de la Cierva Fellow, Department of Aerospace Engineering, Universidad Carlos III de Madrid, Leganés, Spain. gdessena@ing.uc3m.es*

Marco Civera *Tenure-track Assistant Professor, Department of Structural, Geotechnical and Building Engineering, Politecnico di Torino, Turin, Italy. marco.civera@polito.it*

Mikel Janices Chamizo *Graduate Student, Department of Aerospace Engineering, Universidad Carlos III de Madrid, Leganés, Spain. 100512197@alumnos.uc3m.es*

ABSTRACT

System identification (SI) is an important subfield of control engineering. In structural dynamics, SI methods allow for the extraction of modal parameters, thus enabling the dynamic characterisation of structures. Recently, an efficient frequency domain identification method, the Loewner Framework (LF), has been extended to modal parameter extraction. The LF is based on tangential interpolation, and as such, data partitioning is fundamental for its operation. Traditionally, real-valued data is used for the fitting process. This means that complex-valued transfer function measurements are forced into the real domain prior to fitting, resulting in a computational penalty. This work proposes to validate the use of complex-valued data partitioning within structural dynamics to increase the computational efficiency of LF. For this aim, a numerical model of a mass-spring-damper system is modelled; then, its dynamic response is simulated in MATLAB 2024b, while considering different levels of noise. The results show that the complex-valued data sampling identification results perfectly match those using real-valued data, theoretically ought to be better for solving the system realisation problem via tangential interpolation.

Keywords: System Identification, Modal Analysis, Tangential Interpolation, Loewner Framework

1 Introduction

System identification (SI) is, in the broad sense, a subfield of control engineering [1]. The general aim of SI is to identify a system model, parameters, and characteristics. This can be carried out on either numerical or experimental systems, the latter usually being more challenging. Over the years a wide range of methods has been proposed to address this challenge. In particular, many methods target one of the most basic issues in structural dynamics: the identification of modal parameters [2]. Modal analysis, the process of obtaining modal parameters numerically or experimentally, is the backbone of modern structural dynamics as it allows characterisation of the dynamics of a *linear* system, either to gain deeper insight into coupled interactions, such as flutter [3], or to update numerical models, such as in finite element model updating [4].

The main outputs of modal analysis are the modal parameters: natural frequencies (ω_n), damping ratios (ζ_n), and mode shapes ($\boldsymbol{\phi}_n$) [5]. Modal analysis can also be classified by the type and domain of the data used. Data may come from experimental and operational settings. In the former the input is known,

Except where otherwise noted, content of this paper is licensed under a Creative Commons Attribution 4.0 International License.

The reproduction and distribution with attribution of the entire paper or of individual pages, in electronic or printed form, including any material under non-CC-BY 4.0 licenses is hereby granted by the authors and respective copyright owners.

whereas in the latter the system input is unknown [6]. These distinctions give rise to Experimental Modal Analysis (EMA) and Operational Modal Analysis (OMA), respectively. Furthermore, identification can be performed in the time or frequency domain, with the frequency domain for EMA typically relying on frequency response functions (FRFs).

Recently, an efficient identification method known as the Loewner Framework (LF) has been extended to frequency domain EMA [7]. The method is based on tangential interpolation and, for a set of complex-valued numerical or experimental frequency domain data, requires partitioning the target data into two subsets. Frequently, data are transformed into the real number domain before interpolation [8], as explained in later sections, incurring a computational penalty.

The research question addressed here is whether the extra computational effort required to obtain real-valued data is justified when standard transfer functions are inherently complex-valued. To this end, we implement complex partitioning in the latest multiple-input multiple-output (MIMO) implementation of LF, the improved LF (iLF) [9]. We then define a suitable numerical model with 10 degrees of freedom for a mass-spring-damper system in MATLAB R2024b, and use numerical impulse testing to generate displacement and force time histories from which FRFs are computed. The tests include cases with different amplitudes of artificially added white Gaussian noise (AWGN) to evaluate both noise robustness and accuracy of the complex partitioning.

1.1 The Loewner Framework

The Loewner Framework (LF) has its conceptual origins in model order reduction [10, 11]. First deployed for the modelling of multiport circuits in Electrical Engineering [8, 12], it has since been adapted to unsteady aerodynamics within Aeronautical Engineering [13] and, more recently, to the extraction of modal parameters from SIMO mechanical systems for structural health monitoring (SHM) [7]. Its efficiency for system identification via modal parameter extraction was examined in [14]. Subsequent developments extended the LF to output-only settings [15] and to MIMO systems, while also improving computational performance [9]. These advances motivate the adoption of the improved Loewner Framework, iLF, which is the variant considered in this work.

In summary, the LF constructs a rational representation of FRFs, by partitioning the samples into two tangential subsets or directions. From these subsets, rational tangential interpolants are assembled using the Loewner matrix $\mathbb{L}$, introduced by Karl Loewner in the 1930s [16].

Before proceeding, a concise technical overview of the LF—which underpins the computational implementation of the iLF—is presented, beginning with the definition of the Loewner matrix $\mathbb{L}$. *For a row array of pairs of complex numbers* (μ_j, v_j), $j = 1,...,q$, *and a column array of pairs of complex numbers* (λ_i, w_i), $i = 1,...,\rho$, *such that* λ_i, μ_j *distinct, the associated* $\mathbb{L}$ *can be defined:*

$$\mathbb{L} = \begin{bmatrix} \frac{\mathbf{v}_1 - \mathbf{w}_1}{\mu_1 - \lambda_1} & \cdots & \frac{\mathbf{v}_1 - \mathbf{w}_\rho}{\mu_1 - \lambda_\rho} \\ \vdots & \ddots & \vdots \\ \frac{\mathbf{v}_q - \mathbf{w}_1}{\mu_q - \lambda_1} & \cdots & \frac{\mathbf{v}_q - \mathbf{w}_\rho}{\mu_q - \lambda_\rho} \end{bmatrix} \in \mathbb{C}^{q \times \rho} \tag{1}$$

This is valid if a known underlying function $\boldsymbol{\phi}$ *exists, such that* $\mathbf{w}_i = \boldsymbol{\phi}(\lambda_i)$ *and* $\mathbf{v}_j = \boldsymbol{\phi}(\mu_j)$.

Let $\boldsymbol{\Sigma}$ be a linear time invariant system with m inputs, n outputs, and k internal variables, governed by:

$$\begin{aligned} \boldsymbol{\Sigma}: \ \mathbf{E}\frac{d}{dt}\mathbf{x}(t) &= \mathbf{A}\mathbf{x}(t) + \mathbf{B}\mathbf{u}(t) \\ \mathbf{y}(t) &= \mathbf{C}\mathbf{x}(t) + \mathbf{D}\mathbf{u}(t) \end{aligned} \tag{2}$$

Except where otherwise noted, content of this paper is licensed under a Creative Commons Attribution 4.0 International License.

The reproduction and distribution with attribution of the entire paper or of individual pages, in electronic or printed form, including any material under non-CC-BY 4.0 licenses is hereby granted by the authors and respective copyright owners.

where $\mathbf{x}(t) \in \mathbb{R}^k$ is the state, $\mathbf{u}(t) \in \mathbb{R}^m$ is the input and $\mathbf{y}(t) \in \mathbb{R}^p$ is the output. The system matrices are $\mathbf{E}$, $\mathbf{A} \in \mathbb{R}^{k\times k}$, $\mathbf{B} \in \mathbb{R}^{k\times m}$, $\mathbf{C} \in \mathbb{R}^{p\times k}$, and $\mathbf{D} \in \mathbb{R}^{p\times m}$. Its transfer function $\mathbf{H}(s)$ can be defined as:

$$\mathbf{H}(s) = \mathbf{C}(s\mathbf{E} - \mathbf{A})^{-1}\mathbf{B} + \mathbf{D} \tag{3}$$

Next, building on the structure of tangential interpolation, sometimes referred to as rational interpolation in tangential directions, the right (Eq. 4) and left (Eq. 5) interpolation data follow:

$$(\lambda_i; \mathbf{r}_i, \mathbf{w}_i),\ i = 1, \ldots, \rho \qquad \left.\begin{array}{c} \mathbf{\Lambda} = \mathrm{diag}[\lambda_1, \ldots, \lambda_\rho] \in \mathbb{C}^{\rho\times\rho} \\ \mathbf{R} = [\mathbf{r}_1\ \ldots \mathbf{r}_\rho] \in \mathbb{C}^{m\times\rho} \\ \mathbf{W} = [\mathbf{w}_1\ \ldots\ \mathbf{w}_\rho] \in \mathbb{C}^{\rho\times\rho} \end{array}\right\} \tag{4}$$

$$(\mu_j, \mathbf{l}_j, \mathbf{v}_j),\ j = 1, \ldots, q \qquad \left.\begin{array}{c} \mathbf{M} = \mathrm{diag}[\mu_1, \ldots, \mu_q] \in \mathbb{C}^{q\times q} \\ \mathbf{L}^T = [\mathbf{l}_1\ \ldots \mathbf{l}_q] \in \mathbb{C}^{p\times q} \\ \mathbf{V}^T = [\mathbf{v}_1\ \ldots\ \mathbf{v}_q] \in \mathbb{C}^{m\times q} \end{array}\right\} \tag{5}$$

The indices λ_i and μ_j denote, respectively, the sampling locations for the right set $\mathbf{R}$ and the left set $\mathbf{L}$ from which the approximation $\mathbf{H}(s)$ is formed, while ρ and q are their cardinalities. The vectors $\mathbf{w}_i$ and $\mathbf{v}_j$ specify the right and left tangential direction vectors—typically chosen at random in practice [13]–and the quantities $\mathbf{r}_i$ and $\mathbf{l}_j$ are the corresponding right and left tangential data.

Rational tangential interpolation is achieved by determining a transfer matrix $\mathbf{H}(s)$, associated with the realisation $\mathbf{\Sigma}$ in Eq. 2, that enforces the tangential matching conditions along $\mathbf{w}_i$ and $\mathbf{v}_j$. Equivalently, the Loewner pencil built from these data satisfies Eq. 6:

$$\begin{aligned} \mathbf{H}(\lambda_i)\mathbf{r}_i &= \mathbf{w}_i,\ i = 1\ldots., \rho \\ \mathbf{l}_j\mathbf{H}(\mu_j) &= \mathbf{v}_j,\ j = 1, \ldots, q \end{aligned} \tag{6}$$

Now, given a set of points $Z = \{z_1, \ldots, z_N\}$ in the complex plane, the corresponding value of $\mathbf{H}(s)$ can be separated into left $\lambda_{i=1\ldots\rho}$ and right $\mu_{j=1\ldots q}$ data with $N = q + \rho$:

$$\begin{aligned} Z &= \{\lambda_1, \ldots, \lambda_\rho\} \cup \{\mu_1, \ldots, \mu_q\} \\ Y &= \{\mathbf{w}_1, \ldots, \mathbf{w}_\rho\} \cup \{\mathbf{v}_1, \ldots, \mathbf{v}_q\} \end{aligned} \tag{7}$$

Hence, the matrix $\mathbb{L}$ becomes:

$$\mathbb{L} = \begin{bmatrix} \frac{\mathbf{v}_1\mathbf{r}_1 - \mathbf{l}_1\mathbf{w}_1}{\mu_1 - \lambda_1} & \cdots & \frac{\mathbf{v}_1\mathbf{r}\rho - \mathbf{l}_1\mathbf{w}\rho}{\mu_1 - \lambda\rho} \\ \vdots & \ddots & \vdots \\ \frac{\mathbf{v}_q\mathbf{r}_1 - \mathbf{l}_q\mathbf{w}_1}{\mu_q - \lambda_1} & \cdots & \frac{\mathbf{v}_q\mathbf{r}\rho - \mathbf{l}_q\mathbf{w}\rho}{\mu_q - \lambda\rho} \end{bmatrix} \in \mathbb{C}^{q\times\rho} \tag{8}$$

Since $\mathbf{v}_q\mathbf{r}_\rho$ and $\mathbf{l}_q\mathbf{w}_\rho$ are scalars, the Sylvester equation is satisfied by $\mathbb{L}$ in such a fashion:

$$\mathbb{L}\mathbf{\Lambda} - \mathbf{M}\mathbb{L} = \mathbf{LW} - \mathbf{VR} \tag{9}$$

Thus, the *shifted Loewner matrix*, $\mathbb{L}_s$, that is the $\mathbb{L}$ corresponding to $s\mathbf{H}(s)$, can be defined as:

Except where otherwise noted, content of this paper is licensed under a Creative Commons Attribution 4.0 International License.

The reproduction and distribution with attribution of the entire paper or of individual pages, in electronic or printed form, including any material under non-CC-BY 4.0 licenses is hereby granted by the authors and respective copyright owners.

$$\mathbb{L}_s = \begin{bmatrix} \frac{\mu_1 \mathbf{v}_1 \mathbf{r}_1 - \lambda_1 \mathbf{l}_1 \mathbf{w}_1}{\mu_1 - \lambda_1} & \cdots & \frac{\mu_1 \mathbf{v}_1 \mathbf{r}_\rho - \lambda_\rho \mathbf{l}_1 \mathbf{w}_\rho}{\mu_1 - \lambda_\rho} \\ \vdots & \ddots & \vdots \\ \frac{\mu_q \mathbf{v}_v \mathbf{r}_1 - \lambda_1 \mathbf{l}_q \mathbf{w}_1}{\mu_q - \lambda_1} & \cdots & \frac{\mu_q \mathbf{v}_q \mathbf{r}_\rho - \lambda_\rho \mathbf{l}_q \mathbf{w}_\rho}{\mu_q - \lambda_\rho} \end{bmatrix} \in \mathbb{C}^{q \times \rho} \tag{10}$$

Similarly, the Sylvester equation can now be fulfilled as follows:

$$\mathbb{L}_s \Lambda - \mathbf{M} \mathbb{L}_s = \mathbf{L} \mathbf{W} \mathbf{\Lambda} - \mathbf{M} \mathbf{V} \mathbf{R} \tag{11}$$

These Sylvester equations show that the Loewner and shifted Loewner matrices are Cauchy-like [17]. In particular, they may be interpreted as Hadamard products between a Cauchy matrix and low-rank right-hand-side terms, which anticipates the relevance of the data-partition strategy discussed in Section 1.1.1.

Furthermore, following [10], we may set $\mathbf{D} = 0$ without loss of generality, as it does not influence tangential interpolation in the LF. For clarity, we therefore focus on:

$$\mathbf{H}(s) = \mathbf{C}(s\mathbf{E} - \mathbf{A})^{-1}\mathbf{B} \tag{12}$$

A minimal realisation exists if and only if the system is controllable and observable. Assuming the data are sampled from a system whose transfer function is given by Eq. 12, the generalised tangential observability matrix Oq and the generalised tangential controllability matrix $\mathcal{R}\rho$ are obtained from Eqs. 11 and 12 as:

$$O_q = \begin{bmatrix} \mathbf{l}_1 \mathbf{C}(\mu_1 \mathbf{E} - \mathbf{A})^{-1} \\ \vdots \\ \mathbf{l}_q \mathbf{C}(\mu_q \mathbf{E} - \mathbf{A})^{-1} \end{bmatrix} \in \mathbb{R}^{q \times k} \tag{13}$$

$$\mathcal{R}_\rho = \begin{bmatrix} (\lambda_1 \mathbf{E} - \mathbf{A})^{-1}\mathbf{B}\mathbf{r}_1 & \cdots & (\lambda_\rho \mathbf{E} - \mathbf{A})^{-1}\mathbf{B}\mathbf{r}_\rho \end{bmatrix} \in \mathbb{R}^{k \times \rho} \tag{14}$$

Now, combining Eqs. 13 and 14 with, respectively, Eqs. 8 and 10 yields:

$$\begin{aligned} \mathbb{L}_{j,i} = \frac{\mathbf{v}_j \mathbf{r}_i - \mathbf{l}_j \mathbf{w}_i}{\mu_j - \lambda_i} = \frac{\mathbf{l}_j \mathbf{H}(\mu_i)\mathbf{r}_i - \mathbf{l}_j \mathbf{H}(\lambda_i)\mathbf{r}_i}{\mu_j - \lambda_i} = \\ = -\mathbf{l}_j \mathbf{C}(\mu_j \mathbf{E} - \mathbf{A})^{-1}\mathbf{E}(\lambda_i \mathbf{E} - \mathbf{A})^{-1}\mathbf{B}\mathbf{r}_i \end{aligned} \tag{15}$$

$$\begin{aligned} (\mathbb{L}_s)_{j,i} = \frac{\mu_j \mathbf{v}_j - \lambda_i \mathbf{l}\mathbf{w}_i}{\mu_j - \lambda_i} = \frac{\mu_j \mathbf{l}_j \mathbf{H}(\mu_i)\mathbf{r}_i - \lambda_i \mathbf{l}_j \mathbf{H}(\lambda_i)\mathbf{r}_i}{\mu_j - \lambda_i} = \\ = -\mathbf{l}_j \mathbf{C}(\mu_j \mathbf{E} - \mathbf{A})^{-1}\mathbf{A}(\lambda_i \mathbf{E} - \mathbf{A})^{-1}\mathbf{B}\mathbf{r}_i \end{aligned} \tag{16}$$

Thus, for minimal data, where the right and left data have equal length ($p = q$), the following is required:

$$\mathbb{L} = -O_q \mathbf{E} \mathcal{R}_\rho \qquad\qquad \mathbb{L}_s = -O_q \mathbf{A} \mathcal{R}_\rho \tag{17}$$

This leads to the following system matrix assignment:

$$\mathbf{E} = -\mathbb{L}, \qquad \mathbf{A} = -\mathbb{L}_s, \qquad \mathbf{B} = \mathbf{V}, \qquad \mathbf{C} = \mathbf{W} \tag{18}$$

Except where otherwise noted, content of this paper is licensed under a Creative Commons Attribution 4.0 International License.

The reproduction and distribution with attribution of the entire paper or of individual pages, in electronic or printed form, including any material under non-CC-BY 4.0 licenses is hereby granted by the authors and respective copyright owners.

Consequently, the interpolating rational function can be expressed now as:

$$\mathbf{H}(s) = \mathbf{W}(\mathbb{L}_s - s\mathbb{L})^{-1}\mathbf{V} \tag{19}$$

The previous analysis applies to a minimal data setting, a condition rarely satisfied in practice. However, the LF extends naturally to redundant data. To start, assume:

$$\begin{aligned} \operatorname{rank}[\zeta\mathbb{L} - \mathbb{L}_s] &= \operatorname{rank}[\mathbb{L}\ \mathbb{L}_s] = \\ &= \operatorname{rank}\begin{bmatrix}\mathbb{L} \\ \mathbb{L}_s\end{bmatrix} = k,\ \forall\ \zeta \in \{\lambda_j\} \cup \{\mu_i\} \end{aligned} \tag{20}$$

Then, the short (i.e., economy-size) Singular Value Decomposition (SVD) of $\zeta\mathbb{L} - \mathbb{L}_s$ is computed and a selected rank (i.e. the model order) retained:

$$\operatorname{svd}(\zeta\mathbb{L} - \mathbb{L}_s) = \mathbf{Y}\boldsymbol{\Sigma}_l\mathbf{X} \tag{21}$$

where $\operatorname{rank}(\zeta\mathbb{L} - \mathbb{L}_s) = \operatorname{rank}(\boldsymbol{\Sigma}_l) = \operatorname{size}(\boldsymbol{\Sigma}_l) = k$, $\mathbf{Y} \in \mathbb{C}^{q\times k}$ and $\mathbf{X} \in \mathbb{C}^{k\times\rho}$. Further, note that:

$$\begin{aligned} -\mathbf{A}\mathbf{X} + \mathbf{E}\mathbf{X}\boldsymbol{\Sigma}_l &= \mathbf{Y}^*\mathbb{L}_s\mathbf{X}^*\mathbf{X} - \mathbf{Y}^*\mathbb{L}\mathbf{X}^*\mathbf{X}\boldsymbol{\Sigma}_l = \\ &= \mathbf{Y}^*(\mathbb{L}_s - \mathbb{L}\boldsymbol{\Sigma}_l) = \mathbf{Y}^*\mathbf{V}\mathbf{R} = \mathbf{B}\mathbf{R} \end{aligned} \tag{22}$$

and likewise, $-\mathbf{Y}\mathbf{A} + \mathbf{M}\mathbf{Y}\mathbf{E} = \mathbf{L}\mathbf{C}$ such that $\mathbf{X}$ and $\mathbf{Y}$ are the generalised controllability and observability matrices for the system $\boldsymbol{\Sigma}$ with $\mathbf{D} = 0$. After verifying the right and left interpolation conditions, the Loewner realisation for redundant data is as follows:

$$\mathbf{E} = -\mathbf{Y}^*\mathbb{L}\mathbf{X}, \quad \mathbf{A} = -\mathbf{Y}^*\mathbb{L}_s\mathbf{X}, \quad \mathbf{B} = \mathbf{Y}^*\mathbf{V}, \quad \mathbf{C} = \mathbf{W}\mathbf{X} \tag{23}$$

The reader is encouraged to consult [10] for a comprehensive discussion on the LF and to [18] for the progress of the LF in modal analysis[1].

1.1.1 Real- vs Complex-valued Data Partitioning

From the previous Section, a useful interpretation is that the Loewner and shifted Loewner matrices inherit a Cauchy-like structure. This viewpoint is relevant here because the decay pattern of the corresponding Cauchy matrix depends on how the data are partitioned, which in turn affects the numerical efficiency. For this reason, the choice of partition strategy is not merely implementational, but is tied to the matrix structure exploited by the framework. In fact, the LF is based on tangential interpolation; thus, partitioning of the data along two directions is necessary. Three main strategies exist: (i) HALF&HALF, (ii) ODD&EVEN (complex), and (iii) ODD&EVEN (real):

(i) HALF&HALF: Z is split at its midpoint, with the first $N/2$ samples assigned to the right partition $\{\lambda_i\}$ and the second $N/2$ to the left partition $\{\mu_j\}$;
(ii) ODD&EVEN (complex): odd- and even-indexed samples of Z go to the right and left partitions, with the complex-valued frequency domain data used directly;
(iii) ODD&EVEN (real): the same index assignment as (ii), but complex frequency points are paired with their conjugates before partitioning, and the Loewner matrices are mapped to the real domain via a unitary coordinate transformation.

[1]The iLF MATLAB implementation can be found at `https://doi.org/10.5281/zenodo.13863292`

Except where otherwise noted, content of this paper is licensed under a Creative Commons Attribution 4.0 International License.

The reproduction and distribution with attribution of the entire paper or of individual pages, in electronic or printed form, including any material under non-CC-BY 4.0 licenses is hereby granted by the authors and respective copyright owners.

Usually, the ODD&EVEN (real) partition is used in practice [8] as it is expected to give the best interpolation results. This is due to the ODD&EVEN (real) partition magnitude decay of the off-diagonal entries of a Cauchy matrix (C) being faster than the other partitions. This is shown graphically in Fig. 1. As already hinted before, please note that a C is used here to show this, as the Loewner matrices can be obtained by the Hadamard product between a C and low-rank right-hand sides of the Sylvester equation; see [17] for a detailed description of this alternative problem formulation.

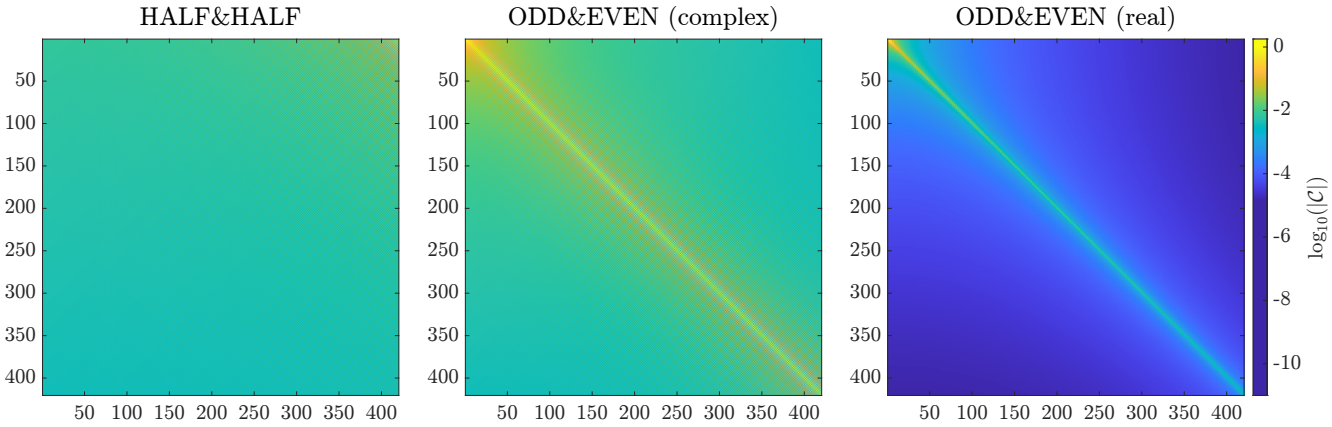

Fig. 1 Absolute value, in logarithmic scale, of a C entries from three data partition methods (replicated from [17]).

The choice of ODD&EVEN (real) data partition seems natural, but, when using complex-valued data, this means that it has to be brought into the real domain, thus adding a computational burden to the LF identification.

The rationale is that, in the present implementation, the main source of computational speed-up is not a generic superiority of complex arithmetic, but the avoidance of realification of complex-valued quantities. Mapping complex FRFs to a real-valued representation increases the effective problem size and therefore enlarges the matrices involved in the Loewner construction and subsequent decompositions. Although complex arithmetic is individually more expensive, the reduced matrix dimensions obtained by working directly with complex-valued data is expected to lead to lower overall computational effort. This effect, and thus the cost-efficiency of the several options, is expected to depend on problem size, rank, and implementation details.

2 Results

In order to assess the viability of ODD&EVEN (complex) data partition, a numerical case study is generated using MATLAB 2024b. The model is a 10 degrees-of-freedom (DoFs) mass-spring-damper system, shown in Fig. 2, where all masses and stiffnesses are of equal value, such that m_n =0.1 kg and k_n =10000 Nm^{-1}. In order to obtain the system dynamic response, the system is excited on the last mass with a unit impulse at the simulation onset. The response is obtained with an in-house developed function based on the classic linear state-space formulation. This accounts for damping, which is modelled using the uncoupled damping assumption by assuming a damping ratio ζ_n = 2% equal for all ten modes. The numerical experiment lasts T_d =60 s, and the resulting displacement time histories are sampled at f_s =512 Hz.

Furthermore, AWGN-corrupted cases are considered as well. The noise levels considered include 0, 1, 2, 5, 7.5, 10, 15, and 20% with the amplitude percentage defined on the (clean) signal's own standard deviation. This means that a total of eight numerical tests are run, such that both input and output are corrupted via AWGN.

The FRF amplitude and phase of selected cases (noise levels of 0, 5, and 20%) are shown in Fig. 3.

Except where otherwise noted, content of this paper is licensed under a Creative Commons Attribution 4.0 International License.

The reproduction and distribution with attribution of the entire paper or of individual pages, in electronic or printed form, including any material under non-CC-BY 4.0 licenses is hereby granted by the authors and respective copyright owners.

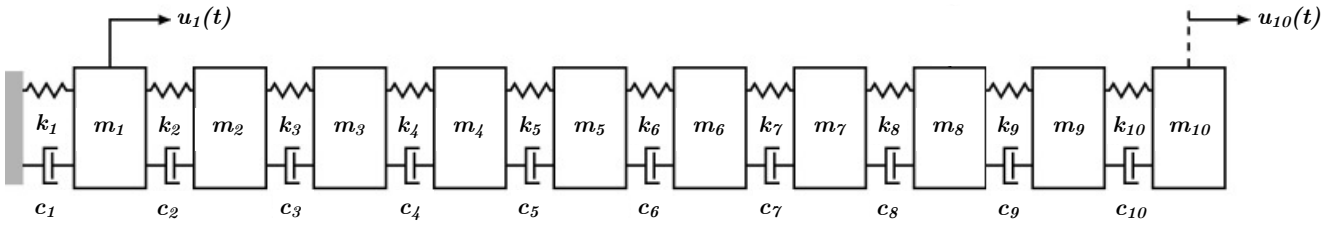

Fig. 2 Schematic of the 10 DoFs mass-spring-damper system (adapted from [19]).

The identification results are compared using the FRF fit from using the two different data partitions and the numerical results, specifically the normalised $\mathcal{H}_2$-error, R^2, and root mean square error (RMSE). Note that the $\mathcal{H}_2$-error is defined as follows:

$$\mathcal{H}_2\text{-error} = \sqrt{\frac{\sum_{j=1}^{N} ||\mathbf{H}_j - \mathbf{H}(i\omega_j)||_F^2}{\sum_{j=1}^{N} ||\mathbf{H}_j||_F^2}} \tag{24}$$

where $||\cdot||_F$ is the Frobenius norm, N is the total number of frequency bins, $\mathbf{H}_j$ is the measured transfer function (the FRF), and $\mathbf{H}(i\omega_j)$ is the transfer function of the model identified via LF. Then, the R^2 is defined as such:

$$R^2 = 1 - \frac{\sum_{j=1}^{N} \left(|\mathbf{H}_j| - |\mathbf{H}(i\omega_j)|\right)^2}{\sum_{j=1}^{N} \left(|\mathbf{H}_j| - \overline{|\mathbf{H}|}\right)^2} \tag{25}$$

where $\bar{\cdot}$ indicates the mean value. Finally, the RMSE is defined as:

$$\text{RMSE} = \sqrt{\frac{1}{N}\sum_{j=1}^{N} \left(\mathbf{H}_j - \mathbf{H}(i\omega_j)\right)^2} \tag{26}$$

The error values computed between the numerical values and the complex-valued iLF are presented in Tab. 1. Note that in Tab. 1, $\mathcal{H}_2$-error and R^2 provide a normalised global discrepancy measure, while RMSE is defined in absolute terms.

Table 1 Relative ($\mathcal{H}_2$-error, R^2) and absolute (RMSE) errors for the different noise levels for the iLF with complex partitioning.

Noise Level [%]	$\mathcal{H}_2$-error	R^2	RMSE
0	0.002	1	1.190e−06
1	0.018	0.999	1.541e−05
2	0.032	0.998	2.812e−05
5	0.075	0.992	6.199e−05
7.5	0.075	0.991	6.594e−05
10	0.116	0.979	9.999e−05
15	0.192	0.936	1.756e−04
20	0.196	0.936	1.764e−04

As shown in Fig. 3, the accuracy of the fit clearly decreases with noise. This is also confirmed in Tab. 1, with the exception of noise levels 15 and 20% where the R^2 values remain almost unchanged.

Except where otherwise noted, content of this paper is licensed under a Creative Commons Attribution 4.0 International License.

The reproduction and distribution with attribution of the entire paper or of individual pages, in electronic or printed form, including any material under non-CC-BY 4.0 licenses is hereby granted by the authors and respective copyright owners.

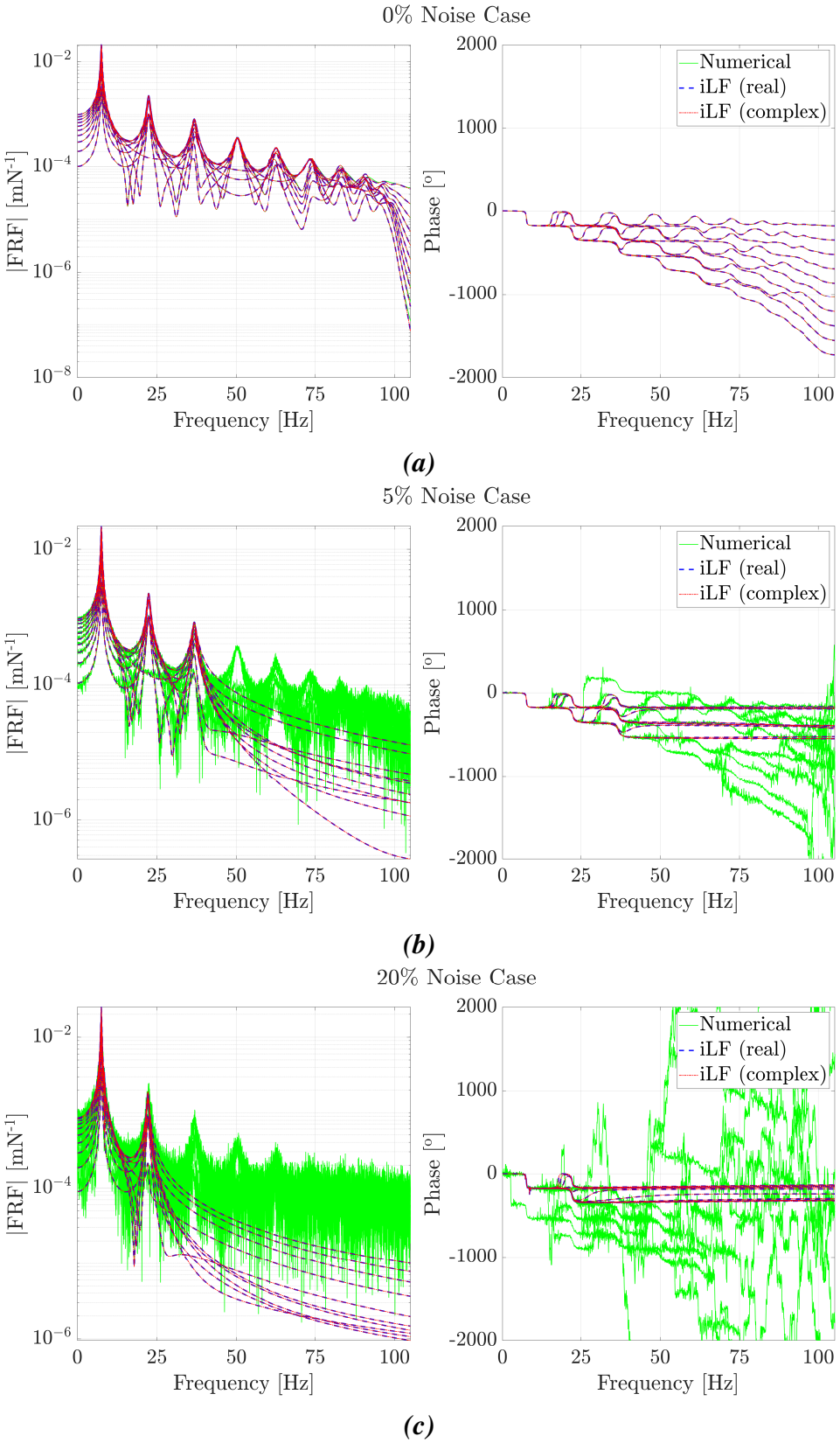

Fig. 3 Fitted and numerical FRFs of the numerical model. (a) 0% noise case, (b) 5% noise case, and (c) 20% noise.

However, the remaining indices still show that noise adversely affects fitting. It should be noted that only the errors of the iLF with complex-valued data fitting are reported in Tab. 1, because they are numerically identical to those obtained with the iLF for real-valued data. This validates the hypothesis of this work,

Except where otherwise noted, content of this paper is licensed under a Creative Commons Attribution 4.0 International License.

The reproduction and distribution with attribution of the entire paper or of individual pages, in electronic or printed form, including any material under non-CC-BY 4.0 licenses is hereby granted by the authors and respective copyright owners.

such that, despite real-valued data partitioning being used for tangential interpolation, complex-valued data partitioning can be used, retaining accuracy. In addition, not forcibly imposing the data to belong to the real domain yields roughly an improvement in computational performance (time to identification) of about one order of magnitude.

3 Conclusions and Future Work

In this work, the use of complex-valued data partition in frequency domain system identification is validated over real-valued data in the specific application to tangential interpolation within the Loewner Framework (LF). The improved LF (iLF) implementation is modified to allow for the use of complex-valued data in the fitting process, and a numerical model of a 10 degrees-of-freedom mass-spring-damper system is used to test its accuracy against the standard (i.e., real-valued) iLF.

Results show how complex-valued data partitioning works as well as real-valued data in the problem under examination. Further validation on more complex and experimental systems is required for generalisation, but this paves the way for an even more computationally efficient implementation of the iLF. Furthermore, the explicit extraction of modal parameters has not been addressed here and remains for future work.

Ongoing research also includes a systematic benchmark against classical complex-plane modal estimators, such as circle-fit-based methods, more realistic measurement noise models (including coloured and low-frequency 1/f components) for numerical studies, as well as broader structural benchmarks with varying stiffness distributions, connection topologies (series and parallel spring connections), and channel layouts, in order to assess the robustness of the proposed partition strategy under more heterogeneous modal scenarios.

Acknowledgments

The first author is supported by grant JDC2024-055593-I funded by MICIU/AEI/10.13039/501100011033 and by ESF+.

Declaration of Use of Artificial Intelligence

Artificial intelligence was not used in the work presented.

References

[1] Lennart Ljung. *System Identification: Theory for the User*. Prentice Hall, 1st edition, 1987. ISBN: 0-13-881640-9.

[2] David J. Ewins. *Modal Testing: Theory, Practice and Application*. Research Studies Press, 2nd edition, 2000. ISBN: 978-0-863-80218-4.

[3] Gabriele Dessena, Alessandro Pontillo, Marco Civera, Dmitry I. Ignatyev, James F. Whidborne, and Luca Zanotti Fragonara. Damping identification sensitivity in flutter speed estimation. *Vibration*, 8:24, 5 2025. ISSN: 2571-631X. doi: 10.3390/vibration8020024.

[4] Gabriele Dessena, Alessandro Pontillo, Dmitry I. Ignatyev, James F. Whidborne, and Luca Zanotti Fragonara. A paradigm shift to assembly-like finite element model updating. *Aerotecnica Missili & Spazio*, 4 2026. ISSN: 0365-7442. doi: 10.1007/s42496-026-00313-8.

Except where otherwise noted, content of this paper is licensed under a Creative Commons Attribution 4.0 International License.

The reproduction and distribution with attribution of the entire paper or of individual pages, in electronic or printed form, including any material under non-CC-BY 4.0 licenses is hereby granted by the authors and respective copyright owners.

[5] Chengyuan Wu, Zhichun Yang, and Shun He. Efficient modal parameter identification using dmd-dbscan and rank stabilization diagrams. *Aerospace Science and Technology*, 161:110112, 6 2025. ISSN: 12709638. doi: 10.1016/j.ast.2025.110112.

[6] Marco Eugeni, Giuliano Coppotelli, Franco Mastroddi, Paolo Gaudenzi, Stephan Muller, and Bernard Troclet. Oma analysis of a launcher under operational conditions with time-varying properties. *CEAS Space Journal*, 10:381–406, 9 2018. ISSN: 1868-2502. doi: 10.1007/s12567-018-0209-5.

[7] Gabriele Dessena, Marco Civera, Luca Zanotti Fragonara, Dmitry I. Ignatyev, and James F. Whidborne. A loewner-based system identification and structural health monitoring approach for mechanical systems. *Structural Control and Health Monitoring*, 2023:1–22, 4 2023. ISSN: 1545-2263. doi: 10.1155/2023/1891062.

[8] Sanda Lefteriu and Athanasios C. Antoulas. Modeling multi-port systems from frequency response data via tangential interpolation. In *2009 IEEE Workshop on Signal Propagation on Interconnects*, pages 1–4, 5 2009. ISBN: 978-1-4244-4490-8. doi: 10.1109/SPI.2009.5089847, `http://ieeexplore.ieee.org/document/5089847/`.

[9] Gabriele Dessena and Marco Civera. Improved tangential interpolation-based multi-input multi-output modal analysis of a full aircraft. *European Journal of Mechanics - A/Solids*, 110:105495, 3 2025. ISSN: 09977538. doi: 10.1016/j.euromechsol.2024.105495.

[10] Andrew J. Mayo and Athanasios. C. Antoulas. A framework for the solution of the generalized realization problem. *Linear Algebra and its Applications*, 425:634–662, 9 2007. ISSN: 00243795. doi: 10.1016/j.laa.2007.03.008.

[11] Athanasios C. Antoulas, Sanda Lefteriu, and A. Cosmin Ionita. *A Tutorial Introduction to the Loewner Framework for Model Reduction*, pages 335–376. Society for Industrial and Applied Mathematics, 7 2017. ISBN: 1545-2263. doi: 10.1137/1.9781611974829.ch8.

[12] Sanda Lefteriu and Athanasios C. Antoulas. A new approach to modeling multiport systems from frequency-domain data. *IEEE Transactions on Computer-Aided Design of Integrated Circuits and Systems*, 29:14–27, 1 2010. ISSN: 02780070. doi: 10.1109/TCAD.2009.2034500.

[13] David Quero, Pierre Vuillemin, and Charles Poussot-Vassal. A generalized state-space aeroservoelastic model based on tangential interpolation. *Aerospace*, 6:9, 1 2019. ISSN: 2226-4310. doi: 10.3390/aerospace6010009.

[14] Gabriele Dessena, Marco Civera, Dmitry I. Ignatyev, James F. Whidborne, Luca Zanotti Fragonara, and Bernardino Chiaia. The accuracy and computational efficiency of the loewner framework for the system identification of mechanical systems. *Aerospace*, 10:571, 6 2023. ISSN: 2226-4310. doi: 10.3390/aerospace10060571.

[15] Gabriele Dessena, Marco Civera, Ali Yousefi, and Cecilia Surace. Next-lf: A novel operational modal analysis method via tangential interpolation. *International Journal of Mechanical System Dynamics*, 5:401–414, 9 2025. ISSN: 2767-1399. doi: 10.1002/msd2.70016.

[16] Karl Löwner. Über monotone matrixfunktionen. *Mathematische Zeitschrift*, 38:177–216, 12 1934. ISSN: 0025-5874. doi: 10.1007/BF01170633.

[17] Davide Palitta and Sanda Lefteriu. An efficient, memory-saving approach for the loewner framework. *Journal of Scientific Computing*, 91:31, 5 2022. ISSN: 0885-7474. doi: 10.1007/s10915-022-01800-3.

[18] Gabriele Dessena and Marco Civera. Modal parameter extraction via the loewner framework: Current progress and future directions. In Michael Döhler, Adrien Mélot, and Manuel López Aenlle, editors, *Proceedings of the 11th International Operational Modal Analysis Conference (IOMAC 2025)*, pages 81–91. International Group of Operational Modal Analysis, 2025. ISBN: 978-84-09-75120-4. `https://hal.science/hal-05232739v1`.

Except where otherwise noted, content of this paper is licensed under a Creative Commons Attribution 4.0 International License.

The reproduction and distribution with attribution of the entire paper or of individual pages, in electronic or printed form, including any material under non-CC-BY 4.0 licenses is hereby granted by the authors and respective copyright owners.

[19] Lawrence A. Bull, Paul A Gardner, Julian Gosliga, Timothy J. Rogers, Nikolaos Dervilis, Elizabeth J. Cross, E. Papatheou, A.E. E. Maguire, C. Campos, and K. Worden. Foundations of population-based shm, part i: Homogeneous populations and forms. *Mechanical Systems and Signal Processing*, 148:107141, 2 2021. ISSN: 08883270. doi: 10.1016/j.ymssp.2020.107141.

Except where otherwise noted, content of this paper is licensed under a Creative Commons Attribution 4.0 International License.

The reproduction and distribution with attribution of the entire paper or of individual pages, in electronic or printed form, including any material under non-CC-BY 4.0 licenses is hereby granted by the authors and respective copyright owners.